Materials Today Bio 28 (2024) 101190

Contents lists available at ScienceDirect

Materials Today Bio

journal homepage: www.journals.elsevier.com/materials-today-bio

Polydopamine-coated polycaprolactone/carbon nanotube fibrous scaffolds loaded with basic fibroblast growth factor for wound healing

Dapeng Cui [a,1], Wei Guo [b,1], Jing Chang [c,1], Shuang Fan [a], Xiaochen Bai [a], Lei Li [a], Chen Yang [a], Chuanlin Wang [c,*], Ming Li [c,**], Jiandong Fei [a,***]

[a] Hepatobiliary Surgery Department, The First Affiliated Hospital of Hebei North University, Zhangjiakou, Hebei, 075000, China
[b] Emergency Department, Peking University People's Hospital, Beijing, 100044, China
[c] Trauma Medicine Center, National Center for Trauma Medicine, Key Laboratory of Trauma and Neural Regeneration (Peking University, Ministry of Education), Peking University People's Hospital, Beijing, 100044, China

ARTICLE INFO

Keywords:
Electrospinning
Electroactive scaffold
Polydopamine surface modification
Basic fibroblast growth factor
Wound healing

Skin is the largest organ in the human body, whose structural integrity plays a significant role in maintaining the stability of the internal environment of human body. However, the repair of large area skin wounds and the healing of chronic skin ulcers are still unsolved clinical problems. In the research, a novel electroactive oriented scaffold composed of polycaprolactone (PCL) and carbon nanotubes (CNT) was prepared by electrospinning method. By using polydopamine (PDA) surface modification which was inspired by mussel, the basic fibroblast growth factor (bFGF) was gently loaded onto the PCL/CNT fiber scaffold, and the PCL/CNT-PDA-bFGF fiber scaffold was obtained, which could release bFGF continuously within 14 days. Fibroblasts were cultured on the scaffolds to evaluate the effect of scaffolds on wound healing in vitro. The effect of these stents on wound healing in vivo was studied using SD rat model of total cortical defect. In addition, the mechanism of the new scaffold promoting wound healing by anti-inflammatory, antioxidant, promoting granulation tissue regeneration and collagen fiber deposition was explored through histological analysis. The results of both in vitro and in vivo experiments indicate that PCL/CNT-PDA-bFGF fiber scaffold can effectively promote skin wound healing. In summary, this study provides a promising novel strategy for skin tissue repair (see Scheme 1).

1. Introduction

As the largest organ of the human body, skin has important functions and plays a significant role, such as protection, excretion, regulation of body temperature, and sensitivity to stimulation [1]. The healing of skin injury is a complicated process, involving four stages: hemostasis, inflammation, proliferation and remodeling [2]. Skin injuries, especially chronic injuries and large area burns, often require long-term treatment [3,4]. This not only causes suffering to patients, but also imposes a huge financial burden on the global healthcare industry. In recent years, with the rapid development of tissue engineering, in order to better promote skin tissue repair, more and more biological materials have been developed, improved, and applied in the field of skin repair.

In cells, electrical signals can regulate cellular behavior and facilitate intercellular communication [5]. Studies have shown that the active endogenous electrical signals around cells are excellent signals for inducing cell proliferation, migration, and promoting tissue repair [6]. Carbon nanotube (CNT) is quantum materials with special structure. Due to its unique conductivity and electrical activity, CNT has gradually attracted people's attention in tissue engineering [7]. In addition, electroactive materials can also promote tissue regeneration and

* Corresponding author.
** Corresponding author.
*** Corresponding author.
E-mail addresses: wangchuanlinvip@163.com (C. Wang), liming_ort@bjmu.edu.cn (M. Li), yfyfeijiandong@163.com (J. Fei).
[1] These authors contributed equally to this work.

https://doi.org/10.1016/j.mtbio.2024.101190
Received 14 May 2024; Received in revised form 18 July 2024; Accepted 5 August 2024
Available online 6 August 2024

functional recovery by regulating the immune microenvironment. Among them, the most significant performance is to promote the transformation of M1 macrophages into M2 macrophages, thereby reducing the expression of inflammatory factors [8]. However, the use of CNT has certain biosafety risks. Studies have shown that dispersing CNT into other substances can reduce the toxic effects of CNT and enhance biosafety [9].

At present, there are various types and forms of materials used in skin tissue repair, such as sponges, hydrogels, powders, and fiber scaffolds [10,11]. Among these, the electrospun nanofiber scaffold, prepared by electrospinning technology has the following outstanding advantages: (1) The fiber diameter is at the nanometer level, smaller than the cell diameter, which can better simulate the structure and biological function of the natural extracellular matrix [12,13]; (2) It has large porosity and specific surface area, allowing it to be combined with other macromolecules to play the role of carriers [14]; (3) Some electrospinning raw materials exhbit good biosafety and degradability, making them suitable for human application and easy absorption [15]. Consequently, the electrospun nanofiber scaffold has gained continuous attention in the field of biomedicine, and has been effectively utilized in wound repair, biological tissue engineering, drug-controlled release and so on. Polycaprolactone (PCL) is a common raw material for creating electrospun nanofiber scaffolds. As a biocompatible material, approved by the FDA for tissue engineering, PCL is characterized by easy processing, high stability, and simple surface modification [16]. By dispersing CNT, as a dispersant, into PCL, the PCL/CNT fiber scaffold would be oriented and electroactive, so it can better simulate the extracellular matrix microenvironment and promote tissue repair and healing [17,18]. On the other hand, it can also reduce the cytotoxicity of CNT and enhance its biocompatibility [9]. For example, Ahmadi et al. prepared PU/Cs/CNT fiber scaffolds for cardiac tissue engineering [19]. Huang et al. added CNT to carboxymethyl chitosan hydrogel to prepare a non-invasive intelligent monitoring scaffold for bone regeneration and monitoring [20]. However, the microenvironment of skin tissue repair is very complex, and it is difficult to meet clinical needs only by PCL/CNT fiber scaffolds without biological activity.

To further enhance the performance of fibrous scaffolds in promoting tissue healing, basic fibroblast growth factor (bFGF) was introduced in this study. bFGF, a spherical protein composed of a single polypeptide, is the most widely used and studied member of the FGF superfamily. It can effectively promote wound healing and tissue regeneration [21], so bFGF is widely used in the field of tissue repair [22]. However, bFGF has a short half-life and rapidly loses its biological activity under normal physiological conditions, resulting in a significant decrease in utilization efficiency [23]. As a novel and effective strategy, using electrospinning technology to bind bFGF to PCL/CNT fiber scaffolds can maintain the activity of bFGF while leveraging the structural advantages of electrospinning scaffolds, resulting in a synergistic effect on promoting tissue healing. However, due to the hydrophobic surface structure of the pure polymer, it is difficult for the protein to attach, resulting in a decrease in loading efficiency.

In recent years, polydopamine (PDA) coating has become a simple, popular and common surface modification method. Inspired by mussels, PDA is a polymer formed from dopamine monomera through self-polymerization reaction, which has good biocompatibility, degradability and adhesion, and can form a uniform and strong covering layer on the material's surface [24]. Its synthesis requirements are simple and mild, and its thickness can be adjusted by changing basic parameters, such as temperature, pH, dopamine concentration and reaction time [25]. In addition, PDA contains a variety of functional groups, such as catecholamines, amines, and imines, providing abundant binding sites for the desired molecules [26]. Protein polypeptides can form covalent bonds with PDA through Michael addition or Schiff reaction under mild reaction conditions, thus achieving efficient loading and slow release of substances [27]. In recent years, PDA, as a polymer coating material, has been widely used in biomolecular delivery systems to enhance the loading efficiency. Cui et al. prepared a PCL fiber scaffolds, which was coated with PDA and loaded with thrombin, to promote wound hemostasis [28]. Pi et al. prepared a PCL/CNT-PDA fiber scaffolds loaded with brain-derived neurotrophic factor to promote peripheral nerve repair [17]. In addition, studies have also demonstrated that PDA has the effect of clearing ROS and reducing inflammation. The rich catecholamine

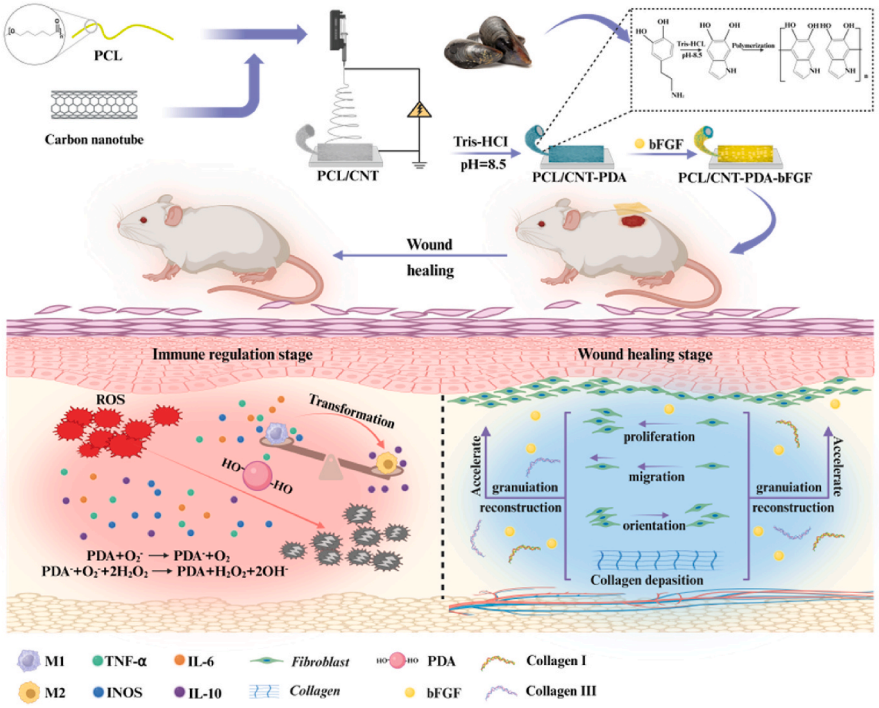

Scheme 1. Preparation of polydopamine-modified electrospinning nanofiber scaffold loaded with basic fibroblast growth factor and its application in wound healing.

groups on the surface of PDA can REDOX reactions with ROS, thus playing an antioxidant role [29]. PDA can also further reduce the damage by trapping free radicals. In addition, PDA can further promote the transformation of macrophages from M1 to M2 by removing ROS, thereby exhibiting anti-inflammatory and immune regulatory properties [30]. For example, Ma et al. developed a microneedle (MN) patch encapsulated in PDA NP to overcome the adverse effects of oxidative stress induced by reactive oxygen species (ROS) on wound healing [30]. Wu et al. developed a polydopamine nanoparticle for relieving early osteoarthritis [29].

In this study, polycaprolactone/carbon nanotube (PCL/CNT) nanofiber scaffolds were prepared using electrospinning technology, and bFGF was loaded onto the scaffolds through PDA surface modification method. First, the microstructure and surface element distribution of the fiber scaffold were observed. The material properties such as water contact angle, electrical conductivity and degradation rate were evaluated. The release spectrum and loading efficiency of bFGF were evaluated by enzyme-linked immunosorbent assay (ELISA). Subsequently, the fibroblasts were cultured on the scaffold to assess the function in wound healing in vitro. The biosafety of fiber scaffolds was evaluated by subcutaneous tissue embedding experiment in rats. Finally, the ability to promote tissue repair of the scaffolds was evaluated in a full-layer skin injury model of SD rats.

2. Materials and methods

2.1. The preparation of the scaffolds

Dissolve 1 g PCL (PCL, 110–120 kDa, Jinan Daigang Co., Ltd., Jinan, China) in 8 mL trifluoroethanol (TFE) (Sigma, USA), and then disperse 0.03 g Carboxyl multi-walled CNTs (MWCNT-COOH) (XFNANO, Nanjing, China) in 2 mL TFE. Then, mix the two kinds of solutions evenly and fill in a 10 mL injection pump. A rotating roller was used to collect the fibers. The electrospinning parameters were fixed as follows: the voltage was15 kV, flow rate was 1 mL/h, roll speed was 1000 rpm, and working distance was 15 cm. At the end of the process, PCL/CNT fiber scaffolds with a thickness of 0.2 mm, were obtained and dried under vacuum overnight at room temperature.

Dissolve the dopamine powder (153.18 Da, McLean Reagent Co., Ltd., Beijing, China) in 10 mM Tris-HCL Buffer (pH = 8.5) to prepare the dopamine solution of 2 mg/mL. Cut the PCL/CNT fiber scaffolds into 12 × 12 mm squares and place in 12-well plates. Each well was added with 1 mL dopamine solution, and soaked on a shaking table at room temperature away from light for 6 h. Then the fiber scaffolds were removed and washed in sterile deionized water 3 times for 5 min each time, and freezing-dried for future use. The sample was named PCL/CNT-PDA.

A solution of bFGF (Solarbio, Beijing, China) with a concentration of 1 μg/mL was prepared. The sterilized PCL/CNT fiber scaffolds and PCL/CNT-PDA fiber scaffolds were respectively placed in 12-well plates. Add 1 mL bFGF solution to each well, soak at room temperature for 12 h, remove the fiber film and freeze dry for future use. The samples were named PCL/CNT-PDA-bFGF and PCL/CNT-bFGF, respectively.

2.2. The characterization of scaffolds

The cross-section of the sample was adhered upward to the sample table with the conductive adhesive. After gold spraying, the structure of the fiber film was observed by field emission scanning electron microscope (SEM, HITACHI SU8010, Tokyo, Japan) at 5 kV accelerated voltage. The energy dispersive spectroscopy (EDS) and element mapping techniques were used to analyze the surface chemical elements of scaffolds. Use Image-Pro Plus 6.0 software (Media Cybernetics, Rockville, MD, USA) to selected 100 nanofibers randomly from samples. Then, the diameter distribution of nanofibers was analyzed. Next, water contact Angle tester (OCA20, DataPhysics, Filderstadt, Germany) was used to measure the water contact angle of PCL/CNT, PCL/CNT-PDA fiber scaffolds. PCL/CNT, PCL/CNT-PDA, PCL/CNT-PDA-bFGF samples (12 × 12 mm) were immersed in phosphate buffered saline (PBS) (pH = 7.4) at 37 °C to determine the degradation rate of the fiber scaffold. After 3 months, the stent was removed, dried under vacuum and weighed. The weight loss was defined as the difference between the original weight and the remaining weight. The ratio of weight loss to original weight is the degradation rate. Each group was independently measured 3 times and a separate sample was used for each data.

2.3. bFGF loading and release assay

To evaluate the distribution and loading capacity of bFGF on PCL/CNT and PCL/CNT-PDA fiber scaffolds, fluorescein isothiocyanate-labeled bovine serum albumin (FITC-BSA) (Solarbio, Beijing, China) was used as a model drug for bFGF. After loading the FITC-BSA, collect the fiber scaffolds, wash it with deionized water, and observe by confocal laser Scanning microscope (CLSM) (TCS-SP8, Leica, Wetzlar, Germany).

PCL/CNT and PCL/CNT-PDA fiber scaffolds were prepared into 12 × 12 mm squares and soaked in 1 mL 1 μg/mL bFGF solution. After standing at room temperature for 12 h, PCL/CNT-bFGF and PCL/CNT-PDA-bFGF fiber scaffold were collected, washed with deionized water, and freeze-dried. The bFGF ELISA kit (Multisciences (Lianke) Biotech Co., Ltd, Hangzhou, China) was uesd to determine the remaining amount of bFGF in the supernatant. The bFGF loading amount was defined as the difference between the original amount and the remaining amount in the supernatant. Then, the load ratio of bFGF is defined as the ratio of the loading amount to the original amount.

To evaluate the release of bFGF, 12 × 12 mm PCL/CNT-bFGF and PCL/CNT-PDA-bFGF fiber scaffold were immersed in 2 mL PBS and shaken with the roll speed of 100 rpm at 37 °C. At day 1, 3, 7, and 14, collect 1 mL supernatant and replaced it with 1 mL PBS. Then, the amount of bFGF in the supernatant was measured by ELISA kit. The release curve of bFGF is drawed according to the change of bFGF cumulative release percentage over time.

2.4. Fibroblast proliferation experiment and morphological observation

The proliferation of L929 cells on PCL/CNT, PCL/CNT-PDA, PCL/CNT-PDA-bFGF scaffolds at day 1, 3, and 5 was measured using CCK8 kit (Dojindo, Tokyo, Japan). After 1, 3, and 5 days of culture, wash the sample with PBS and incubate in 10 % CCK-8 solution. After incubation for 2 h, measure the absorbance of the solution at 450 nm using an enzymoleter (SpectraMaxM2, Molecular Devices, Sunnyvale, CA, USA).

L929 cells were implanted on PCL/CNT, PCL/CNT-PDA, PCL/CNT-PDA-bFGF fiber scaffold. After culturing 3 days, the culture medium was removed. The samples were washed with PBS solution for 3 times, fixed with 3 % glutaraldehyde for 12 h, and dehydrated with gradient alcohol. After gold spraying, the samples were observed by SEM. The cells were stained with 4, 6-diamino-2-phenyllindo (DAPI) (Sigma, USA) and F-actin (Solarbio, China), and observed by confocal laser microscope (OLYMPUS FV1000, Tokyo, Japan).

2.5. Cell migration assay

L929 cells were inoculated into a 96-well plate, and cultured in a constant temperature incubator. After the cells had fully grown, use a sterile gun to evenly scratch the wells. Then the old culture medium was removed and the cells were washed with PBS two to three times until the scratched cells were washed clean. Add the extraction solution and take photos of each group as a 0 h control. Incubate the cells in a 5 % CO_2 incubator. The scratch width was observed, and images were taken at the same position after 24 h and 48 h.

2.6. Cell antioxidant assay

The neutralization ability of free radicals was evaluated by DPPH method. In the initial step, the DPPH solution is prepared in 0.1 mM ethanol. The material was then soaked in a solution, incubated at 37 °C, and shielded from light for half an hour. After incubation, the absorbance level of the sample at 519 nm was measured with the Agilent Cary5000 UV-VIS-NIR spectrophotometer (USA). Clearance rate (%)= (1−Am/As) × 100 %. As represents the initial absorbance of DPPH, while Am represents the absorbance of DPPH after 30 min of sample interaction.

ROS detection kit (Beyotime) was used to evaluate the antioxidant effects of these materials on cells. L929 cells and RAW264.7 cells were inoculated into a 24-well plate containing the material and incubated for 72 h. After incubation, wash the cell with phenol free red DMEM two times, then add 400 μL 50 μM hydrogen peroxide (H_2O_2) to each well for another 2 h. Then, the plate was cleaned twice to remove hydrogen peroxide before adding 10 mM DCFH-DA probe. Incubate the culture dish in the dark for 20 min and wash twice to remove unreacted probes. Observe the intracellular ROS level using a fluorescence microscope and measure the fluorescence intensity. Cell viability was measured by CCK-8 assay.

2.7. Macrophage phenotypic regulation assay

RAW264.7 cells were inoculated onto confocal disks at a density of 3 × 10^4/well. After 12 h of culture, PCL/CNT, PCL/CNT-PDA and PCL/CNT-PDA-bFGF scaffold were added into the corresponding holes, respectively. After continuing the culture for 24 h, remove the material. The cells were then stabilized with 4 % paraformaldehyde for 10 min and washed three times with 500 μL PBS for 3 min each time. Penetration was performed with 0.5 % Triton X-100 within 5 min, then sealed with 1 % bovine serum albumin (BSA) at 37 °C for half an hour. Next, the cells were successively treated with 1 μm Rhodamine labeled phlebocyclin for 30 min, and with 2 μm DAPI for 10 min. Laser confocal microscopy is then used to observe the arrangement of stained cytoskeletal actin.

2.8. Quantitative reverse transcription-Polymerase Chain reaction (qPCR)

After culturing for 5 days, extract the total RNA from L929 cells and RAW264.7 cells using an RNA purification kit (ES Science, Shanghai, China). Then use a reverse transcription kit (ABM, Vancouver, Canada) to reverse transcribe into cDNA. Perform the quantitative real-time PCR on a CFX96TM Real-Time PCR System (Bio-Rad, Hercules, CA, USA) using SYBR Green Real-time PCR Master Mix (TOYOBO, Osaka, Japan). The $2^{-\Delta\Delta Ct}$ method was used to calculate the relative gene expression and gene GAPDH was normalized against the housekeeping. The primers used in this study were shown in Supplementary Material Table S1.

2.9. Biosafety in vivo

All experimental procedures in this study were carried out in accordance with ethical guidelines and approved by the Animal Ethics Committee of Peking University People's Hospital (approval number: 2021PHE067). To evaluate the biocompatibility of the scaffolds in vivo, we conducted animal experiments. First, use pentobarbital sodium to anesthetize the SD rats and remove the hair on the back. Then cut open the back skin, and implant 20 mg sample. In the blank control group, only performe skin incision, and without implanting any material. After 14 days, euthanize the two groups of rats, and collect the samples of organs including liver, heart, lung, spleen and kidney. Then, observe the results of HE staining of these tissues and assess whether the materials caused damage to organs.

2.10. In vivo wound healing experiment

All experimental procedures in this study were carried out in accordance with ethical guidelines and approved by the Animal Ethics Committee of Peking University People's Hospital (approval number: 2021PHE067).

The experimental animals were randomly divided into 4 groups including control group, PCL/CNT group, PCL/CNT-PDA group, and PCL/CNT-PDA-bFGF group, and each group have 6.

After anesthesia, the back hair of the rats was removed, and the skin defect wound with a diameter of 1 cm was made in the middle of the dorsal side with a skin punch. Skin defects were covered with corresponding materials in each group except control group. In order to record the healing process of the wound, the wound was photographed at 0, 3, 7 and 14 days after treatment. The calculation formula of wound healing rate is:

$$\text{Wound healing rate} = (A_0 - A) / A_0 \times 100\%$$

A_0 is defined as the initial wound area and A is defined as the current wound area.

After treatment, the rats were killed on the 7th and 14th day, respectively. The tissues were fixed with phosphate buffered formalin for 24 h, dehydrated, and embedded in paraffin. Cut the paraffin-embedded sample into 5 μm slices, dewax with xylene and dehydrate with gradient alcohol. Then, according to the established protocol, the wound were observed by standard hematoxylin and eosin (HE) staining, and was quantitatively treated. Collagen deposition was observed by Masson staining. Additionally, type I collagen and type III collagen primary antibody were used to incubate with the sections, then the positive staining results were quantitatively counted. Additionally, immunofluorescence staining of TNF-α, IL-6 and ROS were used to evaluate the inflammatory response in tissue.

2.11. Statistical analysis

All data are expressed as mean ± standard deviation (SD). The data was analyzed using SPSS 13.0 statistical software and one-way analysis of variance (ANOVA). *$p < 0.05$, **$p < 0.01$, ***$p < 0.001$ were defined as all statistical tests were significant, ns which meant $p > 0.05$, was defined as no statistical difference in the results.

3. Results

3.1. Characterization of scaffolds

The SEM image, as shown in Fig. 1B, shows that the fibers of the PCL/CNT and PCL/CNT-PDA scaffolds are arranged in a directional manner. The PCL/CNT scaffolds had a smooth surface, while in comparison, the PCL/CNT-PDA scaffolds had a rough surface. In addition, from the surface chemical elements diagram in Fig. 1B, it can be seen that after coating PDA, the content of N increases from 0 % to 5.74 %. The fiber diameter distribution was shown in Fig. 1C and D. It can be seen that after coating PDA, the fiber diameter increases from 1.52 ± 0.8 μm to 1.71 ± 0.71 μm. Furthermore, as shown in Fig. 1E, after coating PDA, the water contact angle significantly decreased from 119.06° ± 4.89°–32.36° ± 2.34° ($p < 0.01$). Additionally, Fig. S1 shows the result of degradation rate of the scaffolds, and it can be seen that the three kinds of fibrous scaffolds all exhibited a degradation rate of about 3 % after 1 months.

3.2. bFGF loading and release properties

Fig. 1F shows that the fluorescence intensity of PCL/CNT-PDA fiber scaffold is much higher than that of PCL/CNT, indicating that more bFGF (FITC-BSA) model proteins are loaded on PCL/CNT-PDA fiber

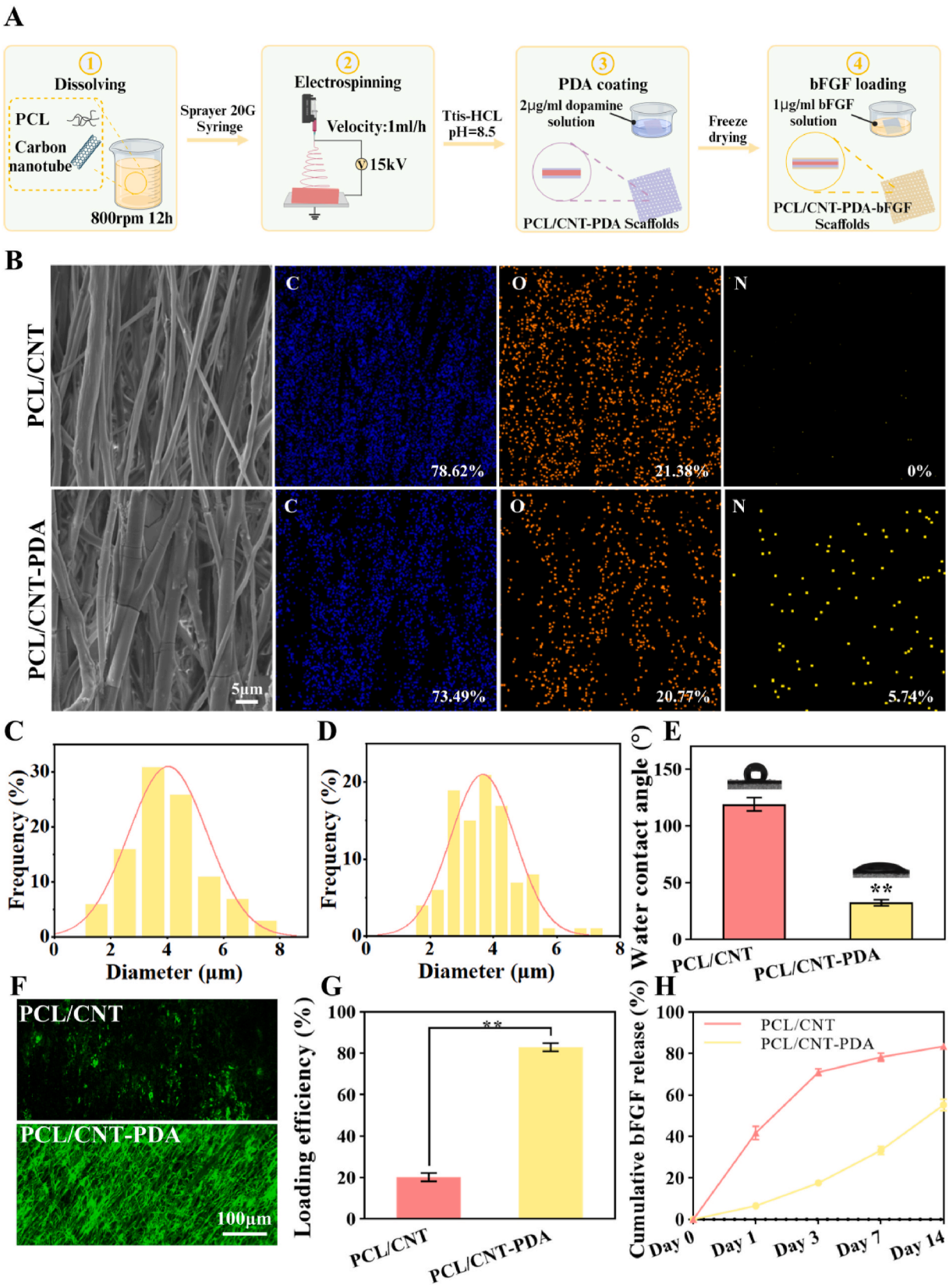

Fig. 1. (A) Cincrete steps for preparing scaffolds. (B) SEM and EDS elemental mapping images of PCL/CNT and PCL/CNT-PDA fibrous scaffolds. Fiber diameter distribution of (C) PCL/CNT and (D) PCL/CNT-PDA. (E) Water contact angles of PCL/CNT and PCL/CNT-PDA fibrous scaffolds (n = 3, **p < 0.01). (F) CLSM images of FITC-BSA loaded onto PCL/CNT and PCL/CNT-PDA scaffolds. (G) Loading efficiency of bFGF on PCL/CNT fibrous scaffolds (n = 5, **p < 0.01). (H) Release kinetics of bFGF from PCL/CNT-bFGF and PCL/CNT-PDA-bFGF scaffolds (n = 3).

scaffold than PCL/CNT. Furthermore, Fig. 1G shows that the loading efficiency of bFGF had a marked increase from 20.29 % ± 1.82 %–82.96 % ± 1.73 % ($p < 0.01$) after coating PDA, which is accordant with the observation of CLSM in Fig. 1F. In addition, the release property of bFGF are shown in Fig. 1H. The PCL/CNT-bFGF fiber scaffold went through a rapid and extensive release phase, and more than 35 % of the load bFGF were released on the first day. After this burst phase, the release from the PCL/CNT-bFGF scaffold significantly slowed down and reached a stable state on day 3. In contrast, no significant burst release was observed in the PCL/CNT-PDA-bFGF fiber scaffold, with approximately 55 % of bFGF released at a relatively stable rate over a 14-day period. This indicates that compared to PCL/CNT, PCL/CNT-PDA can release bFGF more stably and persistently.

3.3. Proliferation and morphology of L929 cells

To evaluate the biosafety of fiber scaffolds in vitro, we conducted cell experiments (Fig. 2A). Fig. 2B shows the detection results of CCK-8, which indicating that L929 cells proliferated continuously on PCL/CNT, PCL/CNT-PDA, and PCL/CNT-PDA-bFGF scaffolds. After culturing for 1 day, there was no significant difference in the proliferation capacity of L929 cells among the three groups ($p > 0.05$). After culturing

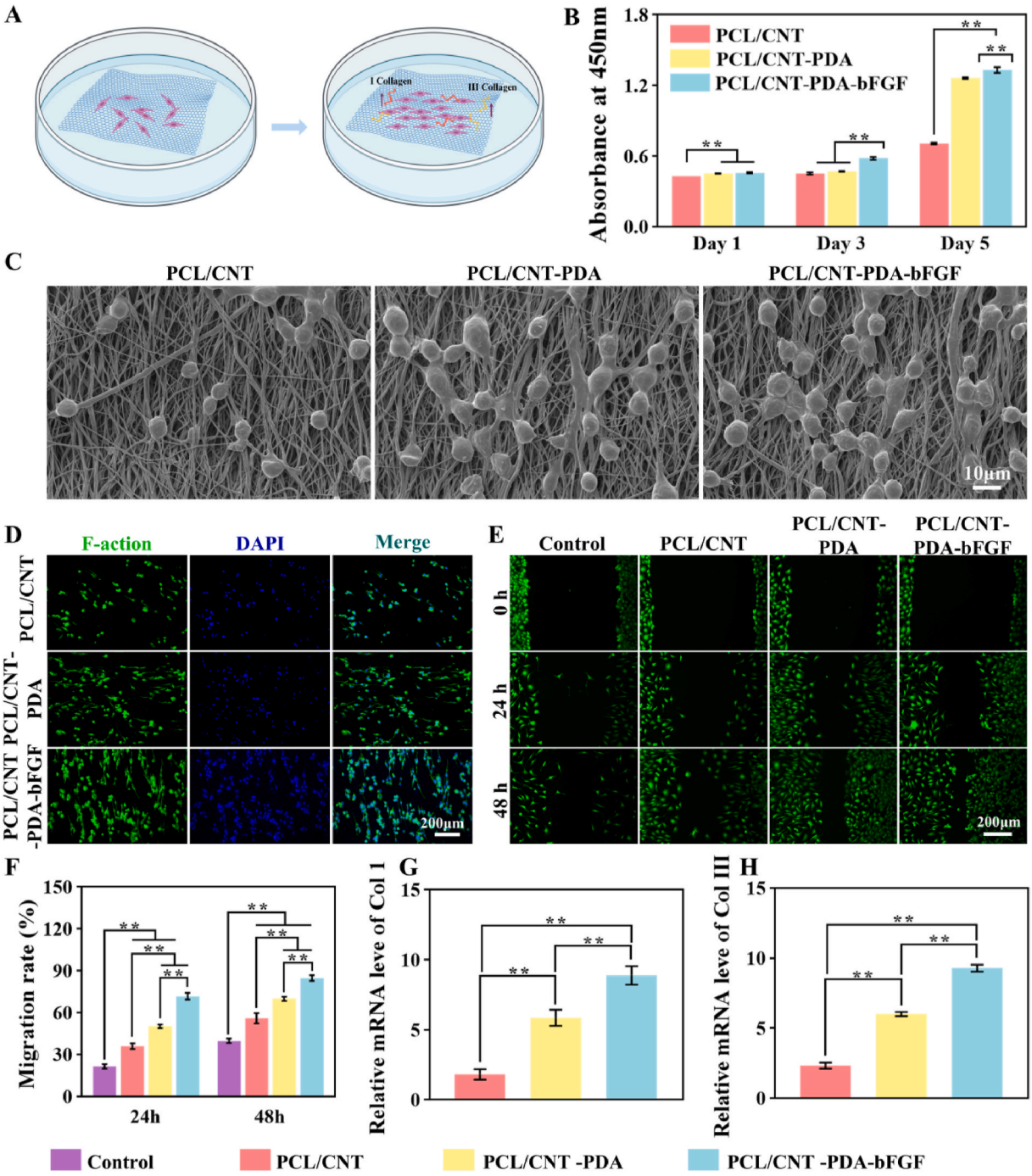

Fig. 2. (A) Schematic diagram of cell co-culture experiment in vitro. (B) Proliferation of L929 cells grown on PCL/CNT, PCL/CNT-PDA and PCL/CNT-PDA-bFGF scaffolds (n = 3, **$p < 0.01$). SEM (C) and CLSM (D) images of L929 cells grown on fibrous scaffolds at 3 days. The cells were stained with F-action (green) and DAPI (blue). CLSM Image (E) of the cell migration experiment and migration rate (F). Relative mRNA expression levels of Col I (G) and Col III (H). (**$p < 0.01$).

for 3 days, the proliferation ability of L929 cells on PCL/CNT-PDA-bFGF scaffold was significantly better than that in the other two groups ($p < 0.01$). After culturing for 5 days, the proliferation ability of L929 cells cultured on PCL/CNT-PDA and PCL/CNT-PDA-bFGF was significantly better than that on PCL/CNT scaffolds ($p < 0.01$). As shown in the SEM image of Fig. 2C, L929 cells adhered to the surface of the scaffold and formed a spindle shape along the fiber axons. From the CLSM image in Fig. 2D, it is obvious that the L929 cell density in PCL/CNT group is much lower than that in other two groups, and PCL/CNT-PDA-bFGF group was significantly better than PCL/CNT-PDA group ($p < 0.01$). The results of the cell migration experiment are shown in Fig. 2E and F. After cultivating for 24 h, the cell migration area of the PCL/CNT-PDA-bFGF group was significantly larger than that of PCL/CNT group and PCL/CNT-PDA group. After cultivating for 48 h, the cell migration area of the PCL/CNT-PDA-bFGF group was still significantly larger than that of the PCL/CNT group and PCL/CNT-PDA group ($p < 0.01$). This result indicates that compared to PCL/CNT and PCL/CNT-PDA, PCL/CNT-PDA-bFGF can better promote cell migration. The PCR results are shown in Fig. 2G and H. The relative mRNA expression levels of Coll I and Coll III in the PCL/CNT-PDA-bFGF group were higher than that of the other two groups ($p < 0.01$).

3.4. Modulation of immune response in vitro

To further explore the mechanism of scaffold promoting wound healing, we evaluated its anti-inflammatory, antioxidant and immune regulating functions (Fig. 3A). The results of DPPH clearance were shown in Fig. 3B, which can be seen that compared to PCL/CNT, PCL/CNT-PDA and PCL/CNT-PDA-bFGF have higher clearance rates, indicating that PCL/CNT-PDA and PCL/CNT-PDA-bFGF have stronger ability to scavenge free radicals. The results of reactive oxygen species staining (DCFH) are shown in Fig. 3C and F. The fluorescence intensity of PCL/CNT-PDA group and PCL/CNT-PDA-bFGF group was significantly lower than that of PCL/CNT group ($p < 0.01$). Similarly, it can be seen from Fig. 3D and E that after treatment with PCL/CNT-PDA and PCL/CNT-PDA-bFGF, the cell viability was higher than that of the H_2O_2 group and PCL/CNT group, indicating that the antioxidant capacity of the fiber membrane was significantly enhanced after PDA coating, which can effectively reduce the damage of ROS to cells. Fig. 3G shows the morphology of macrophages. It can be seen that in the PCL/CNT-PDA and PCL/CNT-PDA-bFGF groups, there was a significant increase in M2 phenotype macrophages, which means that PDA has the great function of regulating the transformation of macrophages from M1 to M2 phenotype. Additionally, the experimental results of PCR showed that the expression levels of pro-inflammatory cytokines TNF-α, iNOS and IL-6 in the PCL/CNT-PDA group and PCL/CNT-PDA-bFGF group were significantly decreased, significantly lower than those in the PCL/CNT group (Fig. 3H–J). At the same time, the anti-inflammatory factor IL-10 in the PCL/CNT-PDA group and PCL/CNT-PDA bFGF group was significantly higher than that in the PCL/CNT group (Fig. 3K).

3.5. Evaluation of wound healing

We established a model of total cortical defect in SD rats to evaluate the effect of PCL/CNT-PDA-bFGF fiber scaffold on wound healing (Fig. 4A). All animal experiments were approved by the People's Medical Ethics Committee of Peking University (Ethics License No.: 2021PHE067). The healing of full-layer skin wounds on day 0, 3, 7, and 14 after surgery, was shown in Fig. 4B–D. It can be seen that at the same time point the healing process of PCL/CNT-PDA-bFGF group was significantly faster than that of other groups. After 7 days of treatment, the wound area was significantly decreased compared with the third day after surgery in each group. After 14 days, the wounds of PCL/CNT-PDA-bFGF group were basically completely healed. PCL/CNT-PDA treated wounds were also almost completely healed, only remaining a very small wound area, while the control group and the PCL/CNT group still had a large wound area. For quantification and visualization, we tracked the dynamic healing process of each group, and the result was shown in Fig. 4C. The quantitative results (Fig. 4D) at each time point also showed that the wound healing rate in PCL/CNT-PDA-bFGF group was higher than that in other groups ($p < 0.01$), which was accordant with the general observation results. It is worth noting that the wound healing rate of PCL/CNT-PDA group was lower than that of PCL/CNT-PDA-bFGF group ($p < 0.01$), indicating that bFGF had a positive effect on wound healing.

3.6. Evaluation of biosafety in vivo

To further evaluate the biosafety of PCL/CNT-PDA-bFGF scaffold in vivo, we conducted subcutaneous embedding experiment. The results in Fig. 5B shows that the other groups didn't show significant foreign body reactions or inflammatory reactions, compared with the control group. To futher evaluate the biotoxic effects on other organs, like lung, heart, liver, spleen and kidney, the results of HE in various organs were compared after 14 days of implantation (Fig. 5C). Histological analysis showed that no significant substantive damage was found in the organs of rats treated with PCL/CNT-PDA-bFGF, meaning that there were no obvious biotoxic effects on the digestive system, respiratory system, circulatory system and metabolic system.

3.7. Histological analysis

HE also was used to discuss the concrete biological mechanism of wound healing. The results in Fig. 4E showed that during the remodeling stage, the PCL/CNT-PDA and PCL/CNT-PDA-bFGF groups achieved reepithelialization and granulation tissue formation, while the wound healing was delayed in the PCL/CNT group and the control group (Fig. 4E). Overall, the thickness of granulation tissue of each group was gradually increased, and the wound length was gradually shortened with wound healing, among which the PCL/CNT-PDA-bFGF group showed the most obvious statistical trend. The quantitative statistics in Fig. 4F and G also confirmed the results of HE staining. Furthermore, the wound length of PCL/CNT-PDA-bFGF group was significantly lower than that of other groups ($p < 0.01$). In addition, compared with the other groups, the PCL/CNT-PDA-bFGF group developed more new granulation tissue and a more complex epidermal structure at day 14, as well as tissue resembling skin appendages. It is suggested that PCL/CNT-PDA-bFGF group can significantly heal the wound, and the healing time is short.

Masson staining showed that the collagen deposition in PCL/CNT-PDA-bFGF fiber scaffold group was extensive and orderly compared with others. More new hair follicles appeared in PCL/CNT-PDA-bFGF group (Fig. 6E). This suggests that the PCL/CNT-PDA-bFGF fiber scaffold improves ECM remodeling capability (Fig. 6B). Coll I and Coll III are the main types of collagen that are involved in the skin repair. The immunohistochemical staining results of Col I and Col III were shown in Fig. 6C and D. The deposition of Coll I and Coll III in all stent groups increased with time, and the collagen expression was higher than that in control group ($p < 0.01$). The expressions of both kinds of collagen in PCL/CNT-PDA-bFGF group were higher than that in other groups, followed by PCL/CNT-PDA group, which was also significantly higher than that in control group and PCL/CNT group ($p < 0.05$) (Fig. 6F and G). As is well known, the enrichment of collagen is beneficial for matrix remodeling and wound healing. These results suggest that the PCL/CNT-PDA-bFGF group can promote wound healing by accelerating the deposition and remodeling of the two kinds of collagen.

The immunofluorescence staining and fluorescence statistical analysis results of TNF-α, IL-6 and ROS are shown in Fig. 7. On day 7 and 14, the fluorescence intensity of TNF-α and IL-6 in PCL/CNT-PDA group and PCL/CNT-PDA-bFGF group was lower than that of the PCL/CNT group (Fig. 7E and F). That means that, PCL/CNT-PDA and PCL/CNT-PDA-bFGF have better anti-inflammatory properties and can reduce

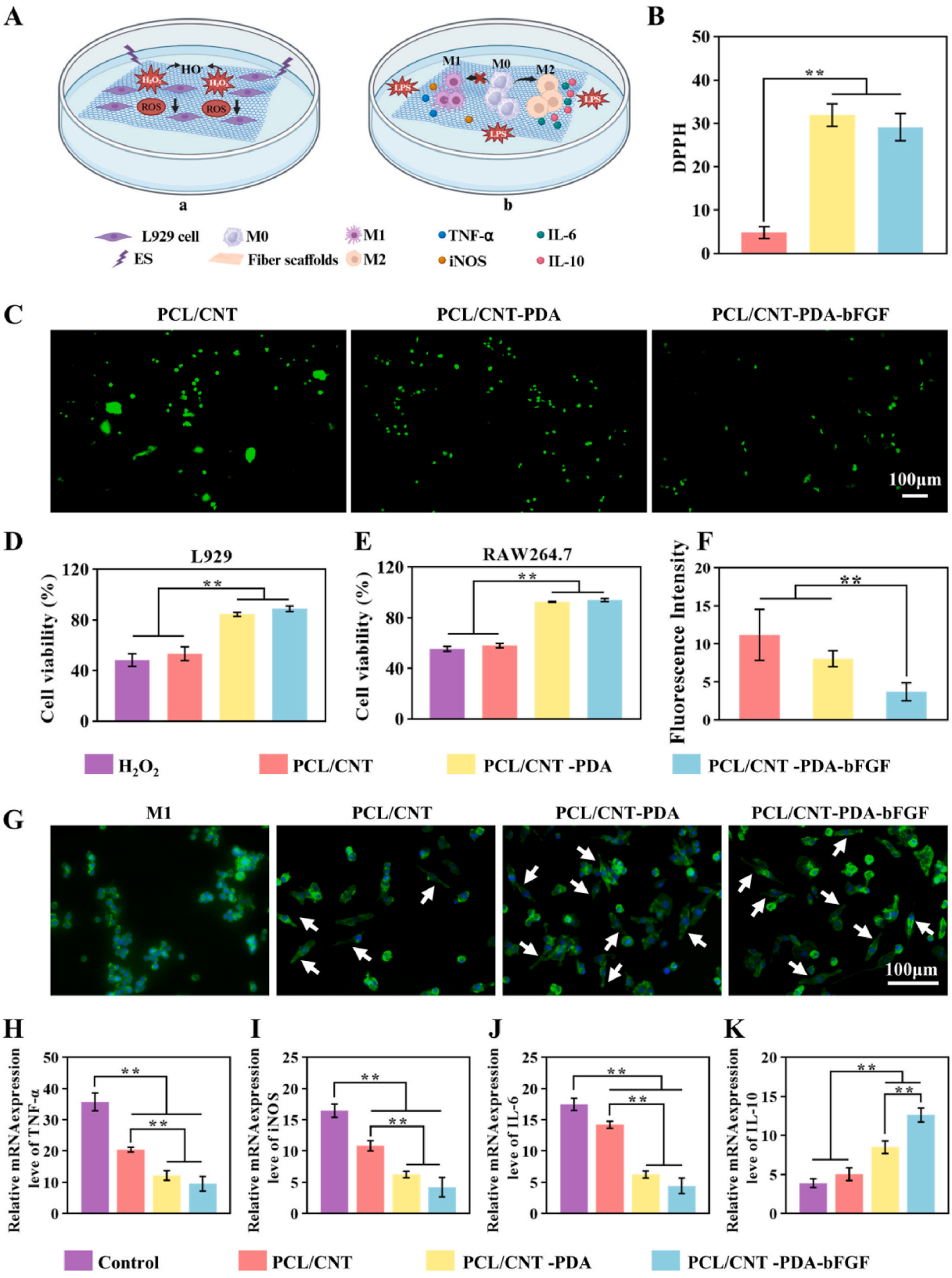

Fig. 3. (A) Schematic diagram of immune regulation. (B) The clearance rate of DPPH. Typical images (C) and fluorescence intensity (F) of reactive oxygen staining (DCFH) of L929 cells. Cell viability of L929 cells (D) and RAW264.7 cells (E) after H_2O_2 induction and different treatments. (G) Morphological changes of macrophages (arrow: M2 macrophages). Relative mRNA expression levels of TNF-α (H), iNOS (I), IL-6 (J) and IL-10 (K). (**p < 0.01).

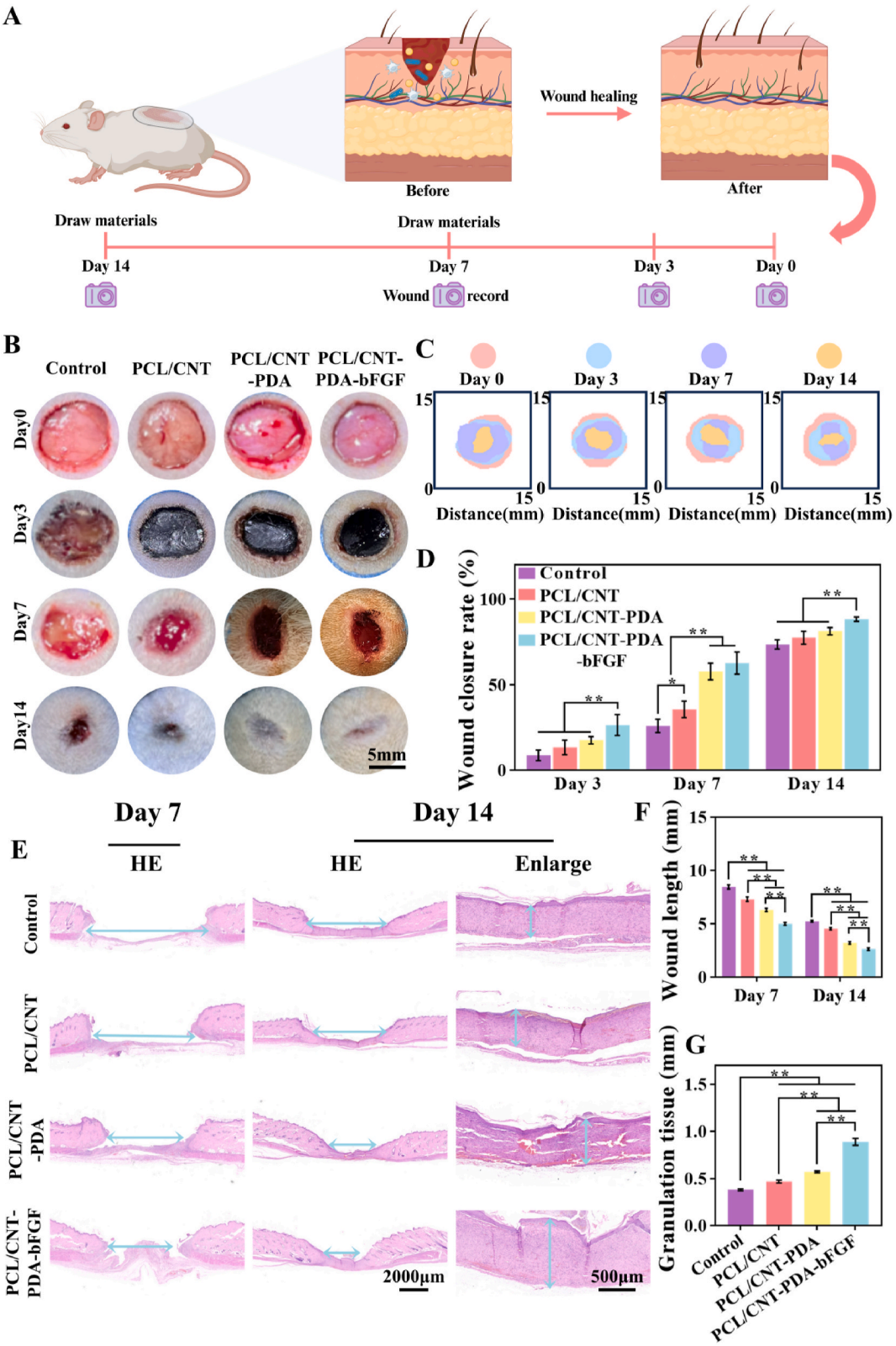

Fig. 4. (A) Schematic diagram of accelerating wound healing based on PCL/CNT-PDA-bFGF scaffolds. (B) The representative photographs of wound in different treatment groups on day 0, 3, 7 and 14. (C) The quantitative and visualized wound trace of these groups. (D) The wound closure rates from different groups on day 0, 3, 7 and 14. (E) Typical images of HE staining (Horizontal arrows: wound length. Vertical arrows: granulation tissue thickness.). The wound length (F) and the granulation tissue thickness (G) in the HE staining. (**p < 0.01).

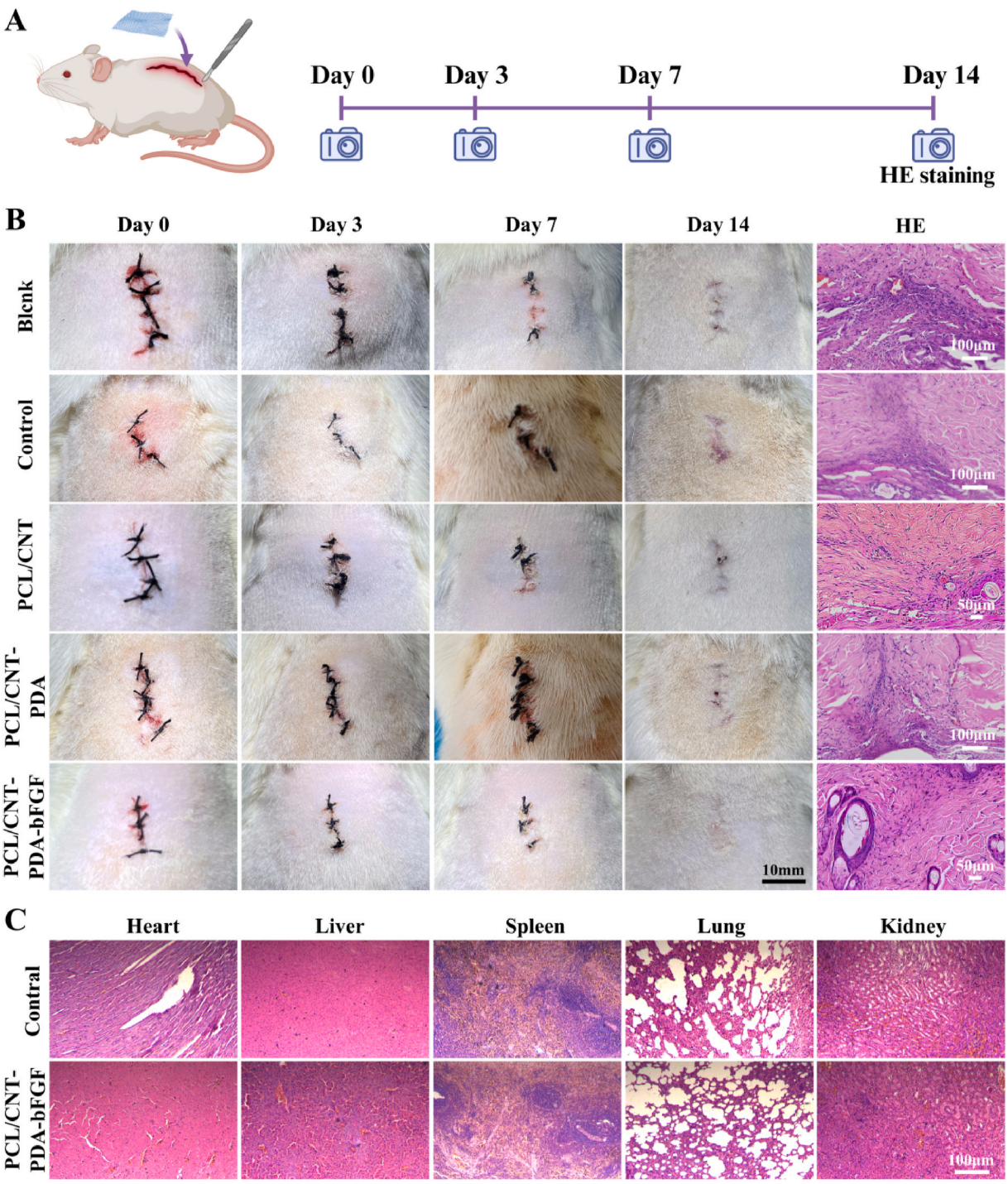

Fig. 5. (A) Schematic diagram of embedding experiment in vivo. (B) Photos of wounds on the 0th day, 3rd day, 7th day and 14th day after surgery. (C) The representative HE staining images of the rat organs (lung, heart, liver, spleen, kidney) after 14 days of embedding.

inflammatory reactions in tissues. Similarly, from the quantitative analysis results of ROS (Fig. 7G), it can be seen that compared to the PCL/CNT group, the PCL/CNT-PDA group and PCL/CNT-PDA-bFGF group have lower ROS fluorescence intensity, indicating that PCL/CNT-PDA and PCL/CNT-PDA-bFGF have a stronger ability to clear ROS in vivo.

4. Discussion

The integrity of skin structure plays a significant role in maintaining the normal physiology of the human body. However, the repair of skin injury, especially the healing of large area skin injury, is still a difficult problem to be solved clinically [31,32]. In this study, PCL/CNT electrospun nanofiber scaffolds were prepared using the electrospinning technique, and basic fibroblast growth factor (bFGF) was loaded onto the scaffold through PDA surface modification. In this way, PCL/CNT-PDA-bFGF scaffold was prepared to use in the field of skin tissue repair.

Electrospun fiber scaffold is widely used in tissue engineering due to its advantages, like small fiber diameter, large specific surface area, high porosity, easy preparation and application [33–35]. In this study, PCL/CNT-PDA-bFGF fiber scaffold was prepared. Among them, PCL is

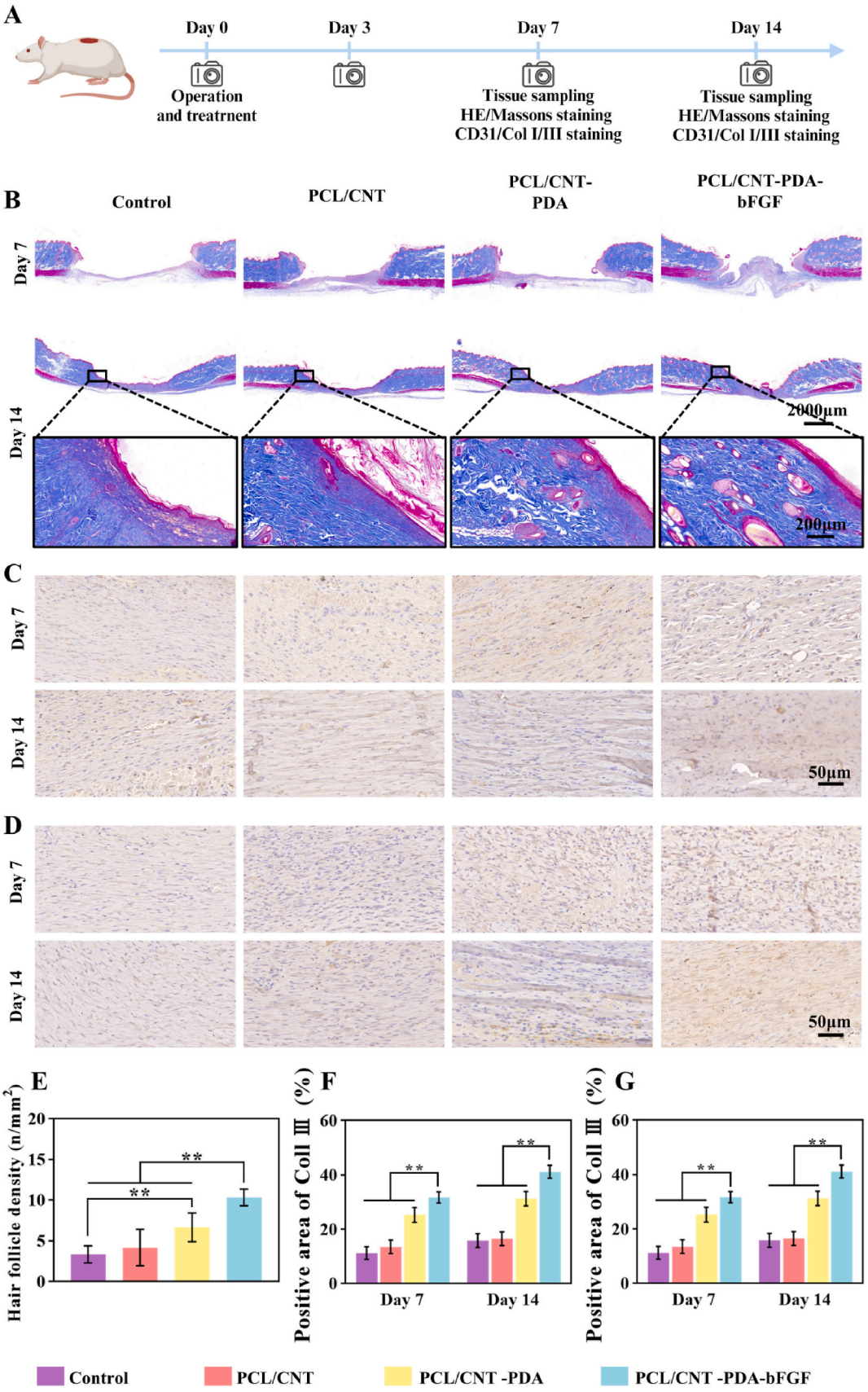

Fig. 6. (A) Flow diagram of wound healing experiment in vivo. (B) Typical images of Masson staining on day 7 and 14. Immumohistochemical staining of collagen I (C) and collagen III (D) in regeneration tissues on day 7 and 14. Quantification of hair follicle density (E), collagen I (F) and collagen III (G) positive area. (**$p < 0.01$).

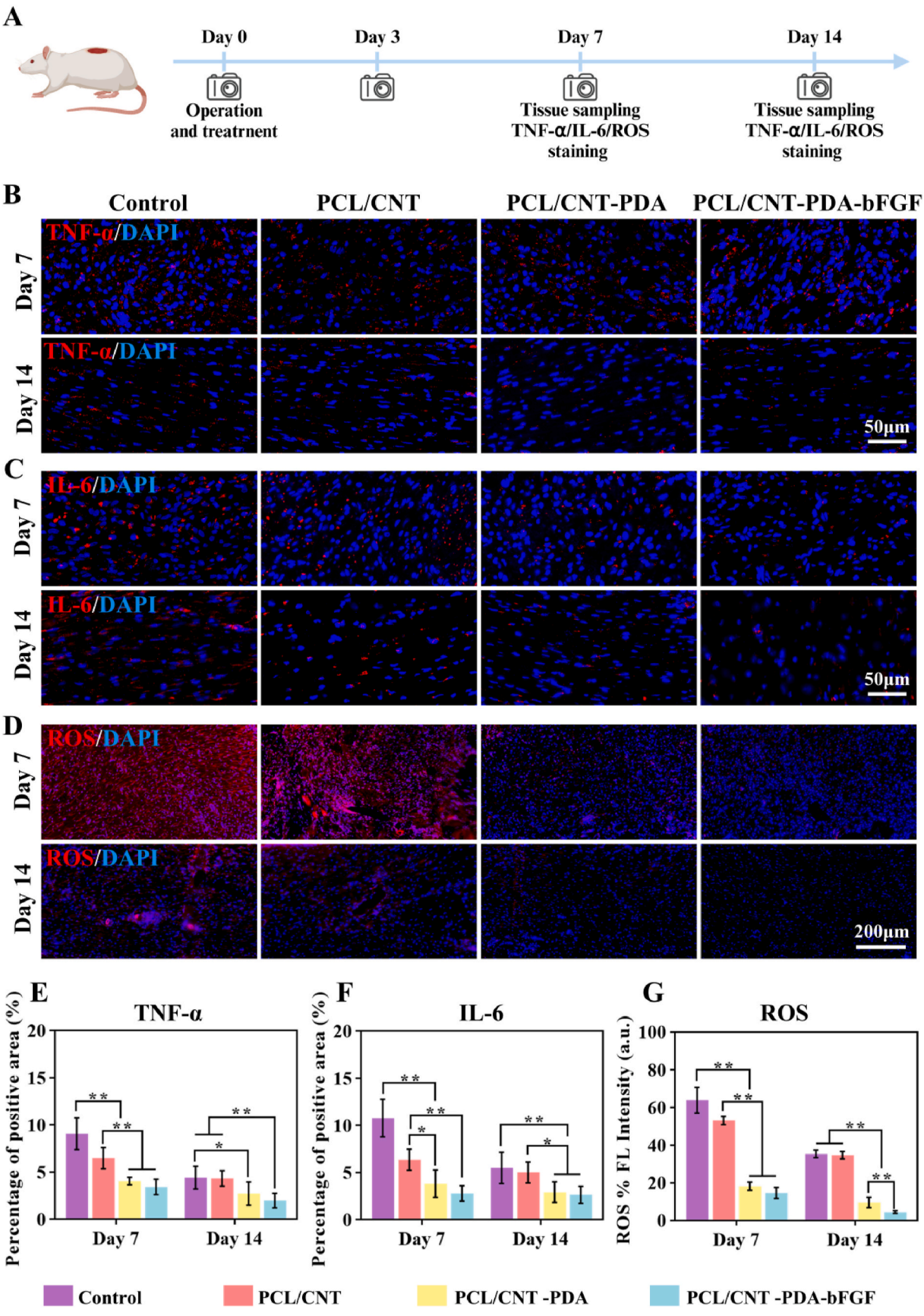

Fig. 7. (A) Flow diagram of wound healing experiment in vivo. Immumohistochemical staining of TNF-α (B) and IL-6 (C) in regeneration tissues on day 7 and 14. Immumohistochemical staining of ROS (D) in regeneration tissues on day 7 and 14. Quantification of TNF-α (E) and IL-6 (F) positive area. (G) Quantitative analysis of ROS. (*$p < 0.05$, **$p < 0.01$).

one of the commonly used raw material for electrospun fiber scaffold. CNT is one of the emerging electroactive biomaterial that can conduct electrical, electrochemical, and electromechanical stimulation to cells [36,37]. Due to its unique electrical activity, CNT is widely used to improve the arrangement of cells and make them closer to normal human tissues, thereby accelerating up tissue healing [38]. Secondly, in order to further enhance the ability of the scaffold to promote tissue healing, the PCL/CNT-PDA fiber scaffold was loaded with bFGF. bFGF is an endogenous polypeptide growth factor with high affinity for heparin, which can promote cell proliferation and migration and promote tissue healing [39]. In addition, in order to improve the loading rate of bFGF, the hydrophobic structure of PCL/CNT polymer surface was modified by coating with PDA. PDA is a biomimetic polymer with high adhesion, biocompatibility and degradability, which can form a stable and adjustable thickness PDA coating on the material surface [40,41]. At the same time, there are many functional groups on the surface of PDA, such as amino groups, carboxyl groups, catechol, etc., which are easy to form coupling with the protein part, and improve the loading rate and achieve the slow and lasting release while maintaining the activity of the protein [42]. The test results showed that the water contact angle of PCL/CNT-PDA was obviously smaller than that of PCL/CNT, and the loading rate of bFGF was obviously higher than that of PCL/CNT, which indicates that the hydrophilicity and loading performance of the materials coated with PDA were significantly improved. The results of bFGF release curve show that PCL/CNT-bFGF fiber scaffold has an obvious bFGF abrupt release stage. In contrast, PCL/CNT-PDA-bFGF can release bFGF more stably and sustainably. In addition, by coating with PDA to improve the hydrophilicity and the loading rate of bFGF, the adhesion and proliferation of cells were promoted additionally, which is conducive to tissue regeneration.

The biocompatibility of the scaffold is also an important factor influencing tissue regeneration [43,44]. The ideal scaffold should possess biodegradability while maintaining biological activity and promoting the adhesion, proliferation and differentiation of cells [23,38,45]. In PCL/CNT-PDA-bFGF scaffold, PCL, PDA and bFGF all have good biocompatibility, which has been widely acknowledged. However, the biocompatibility of CNT depends on a number of factors. Many studies have shown that incorporating other materials with CNT could significantly reduce its toxicity and improve the biocompatibility [36,46–48]. In order to further accurately evaluate the biosafety performance of the material, in this study, fibroblast coculture tests in vitro and embedding tests in vivo were carried out. The results demonstrated that the scaffold prepared in the study exhibited excellent biocompatibility.

Macrophages play an important role in the immune system, playing an important regulatory role in the microenvironment of wound repair. During the process of damage repair, macrophages are mainly inflammatory phenotype (M1) at the beginning, which plays the role of clearing damaged tissues. Subsequently, it was then converted to an anti-inflammatory phenotype (M2) that promotes wound healing [49]. However, this process may cause excessive oxidative stress and inflammatory storms when tissues are damaged, impeding the transition from M1 phenotype to an M2 phenotype, and hindering the progression of subsequent wound regeneration. The results show that the PCL/CNT-PDA-bFGF scaffold can effectively functions as an anti-inflammatory and antioxidant role. On the one hand, PDA plays an antioxidant role by engaging in the REDOX reactions between ROS and the abundant catecholamine groups on the surface, trapping reactive oxygen species, and promoting the transformation of macrophages from M1 to M2. On the other hand, CNT, as an electroactive material, can also promote the transformation of macrophages from M1 to M2 and regulate the immune microenvironment. The combined effect of the two materials equips the scaffold with anti-inflammatory and antioxidant properties.

In order to further evaluate the ability of composite materials in promoting tissue healing, this study conducted a full-layer skin injury model of SD rats, and the test results showed that compared with the other groups, the rats treated with PCL/CNT-PDA-bFGF had a narrower scar width, thicker granulation tissue, and more new hair follicles, indicating that the PCL/CNT-PDA-bFGF indeed had a more rapid and effective ability to promote tissue healing. In addition, to verify the positive effects of PCL/CNT-PDA-bFGF fiber membrane on anti-inflammatory and antioxidant, cell antioxidant assays and immunofluorescence staining of IL-6 and TNF-α were conducted. The results showed that PCL/CNT-PDA-bFGF can effectively reduce the levels of ROS in cells and the content of inflammatory factors in tissues, which means that the fiber scaffold can alleviate inflammation and oxidative damage effectively. The good performance of PCL/CNT-PDA-bFGF in tissue repair is attributed to the following mechanisms: (1) In this study, the material existed in the form of nanofiber which was characterized by small diameter and high porosity, and was conducive to promote rapid tissue repair, through simulating the microenvironment of extracellular matrix and providing matrix platform for tissue repair [50,51]. (2) Due to the addition of CNT, PCL/CNT-PDA-bFGF fiber scaffold had electrical activity, which made the cells arrange according to the shape of the fibers and better simulate the arrangement of normal tissue cells [18]. (3) In addition, coating with PDA, the hydrophilicity of the polymer was significantly increased, which was conducive to maintaining a moist environment of the wound and accelerating tissue recovery [45]. (4) PDA can effectively remove ROS and promote the transformation of macrophages from M1 to M2. At the same time, CNT, as an electroactive material, can also effectively promote the transformation of M1 to M2, thus endowing the PCL/CNT-PDA-bFGF scaffold with good anti-inflammatory and antioxidant effects. These mechanisms work together at the wound site to promote tissue regeneration and repair.

In this study, PCL/CNT-PDA-bFGF fiber scaffold was prepared by electrospinning technology, and it was proved that the scaffold had good tissue healing and biosafety performance. However, there are still some aspects to be improved: (1) The animal model used in this study was SD rat, and no other animals were used for further performance evaluation; (2) The small number of animal samples may lead to a certain bias in the results.

5. Conclusions

In this study, PCL/CNT-PDA-bFGF fiber scaffolds were prepared and the effect on wound healing was evaluated by in vitro and in vivo assays. In vitro, PCL/CNT-PDA-bFGF fiber scaffold can significantly promote the adhesion and proliferation of fibroblasts. In vivo, PCL/CNT-PDA-bFGF fiber scaffolds can effectively promote the granulation tissue regeneration and collagen fiber deposition to promote wound healing. It's considered that the function of PCL/CNT-PDA-bFGF scaffolds is the result of a combination of multiple favorable factors, including the electrical conductivity, regular fiber orientation, PDA surface modification, anti inflammatory, antioxidant, and stable bFGF release. In conclusion, the PCL/CNT-PDA-bFGF fiber scaffold can be considered as a promising material to apply to the skin tissue repair engineering.

Funding

This work was supported by the Hebei Province finance department project, China [grant number ZF2023241], the Health Innovation Special Project of Hebei Provincial Key R&D Program, China [grant numbers 223777101D], the Beijing Natural Science Foundation, China [grant number 7232185], the Natural Science Foundation of China [grant number 81901251] and the National Key R&D Program of China [grant number 2022YFC3006200].

Institutional review Board statement

The study was conducted according to the guidelines of the Declaration of Helsinki, and ap-proved by the Animal Ethics Committee of Peking University People's Hospital (approval num-ber: 2021PHE067).

CRediT authorship contribution statement

Dapeng Cui: Writing – original draft, Visualization, Methodology, Investigation, Funding acquisition, Conceptualization. **Wei Guo:** Writing – original draft, Visualization, Methodology, Investigation, Funding acquisition, Formal analysis, Data curation, Conceptualization. **Jing Chang:** Writing – review & editing, Writing – original draft, Visualization, Methodology, Investigation, Formal analysis, Data curation. **Shuang Fan:** Writing – review & editing, Validation. **Xiaochen Bai:** Writing – review & editing, Validation. **Lei Li:** Validation. **Chen Yang:** Validation. **Chuanlin Wang:** Supervision, Project administration, Funding acquisition, Conceptualization. **Ming Li:** Supervision, Software, Resources, Project administration, Funding acquisition, Conceptualization. **Jiandong Fei:** Supervision, Project administration, Funding acquisition, Conceptualization.

Declaration of competing interest

The authors declare that they have no known competing financial interests or personal relationships that could have appeared to influence the work reported in this paper.

Data availability

Data will be made available on request.

Appendix A. Supplementary data

Supplementary data to this article can be found online at https://doi.org/10.1016/j.mtbio.2024.101190.

References

[1] C. Korupalli, H. Li, N. Nguyen, F.L. Mi, Y. Chang, Y.J. Lin, H.W. Sung, Conductive materials for healing wounds: their incorporation in electroactive wound dressings, characterization, and perspectives, Adv Healthc Mater 10 (2021) e2001384.

[2] O. Castano, S. Perez-Amodio, C. Navarro-Requena, M.A. Mateos-Timoneda, E. Engel, Instructive microenvironments in skin wound healing: biomaterials as signal releasing platforms, Adv. Drug Deliv. Rev. 129 (2018) 95–117.

[3] R. Li, K. Liu, X. Huang, D. Li, J. Ding, B. Liu, X. Chen, Bioactive materials promote wound healing through modulation of cell behaviors, Adv. Sci. 9 (2022) e2105152.

[4] S. Qian, B. Zhao, J. Mao, Z. Liu, Q. Zhao, B. Lu, X. Mao, L. Zhang, L. Cheng, Y. Zhang, W. Cui, X. Sun, Biomedical applications of Janus membrane, Biomedical Technology 2 (2023) 58–69.

[5] S. Martino, F. D'Angelo, I. Armentano, J.M. Kenny, A. Orlacchio, Stem cell-biomaterial interactions for regenerative medicine, Biotechnol. Adv. 30 (2012) 338–351.

[6] S. Parandeh, N. Etemadi, M. Kharaziha, G. Chen, A. Nashalian, X. Xiao, J. Chen, Advances in triboelectric nanogenerators for self-powered regenerative medicine, Adv. Funct. Mater. 31 (2021).

[7] G. Jin, G. Kim, The effect of sinusoidal AC electric stimulation of 3D PCL/CNT and PCL/beta-TCP based bio-composites on cellular activities for bone tissue regeneration, J. Mater. Chem. B 1 (2013) 1439–1452.

[8] Q. Wang, H. Wang, Y. Ma, X. Cao, H. Gao, Effects of electroactive materials on nerve cell behaviors and applications in peripheral nerve repair, Biomater. Sci. 10 (2022) 6061–6076.

[9] E. Niezabitowska, J. Smith, M.R. Prestly, R. Akhtar, F.W. von Aulock, Y. Lavallee, H. Ali-Boucetta, T.O. McDonald, Facile production of nanocomposites of carbon nanotubes and polycaprolactone with high aspect ratios with potential applications in drug delivery, RSC Adv. 8 (2018) 16444–16454.

[10] S. Zhou, Q. Wang, A. Huang, H. Fan, S. Yan, Q. Zhang, Advances in skin wound and scar repair by polymer scaffolds, Molecules 26 (2021).

[11] V. Vijayakumar, S.K. Samal, S. Mohanty, S.K. Nayak, Recent advancements in biopolymer and metal nanoparticle-based materials in diabetic wound healing management, Int. J. Biol. Macromol. 122 (2019) 137–148.

[12] L. Dejob, B. Toury, S. Tadier, L. Gremillard, C. Gaillard, V. Salles, Electrospinning of in situ synthesized silica-based and calcium phosphate bioceramics for applications in bone tissue engineering: a review, Acta Biomater. 123 (2021) 123–153.

[13] X. Fu, J. Wang, D. Qian, L. Xi, L. Chen, Y. Du, W. Cui, Y. Wang, Oxygen atom-concentrating short fibrous sponge regulates cellular respiration for wound healing, Advanced Fiber Materials 5 (2023) 1773–1787.

[14] J. Hong, M. Yeo, G.H. Yang, G. Kim, Cell-electrospinning and its application for tissue engineering, Int. J. Mol. Sci. 20 (2019).

[15] J. Xing, M. Zhang, X. Liu, C. Wang, N. Xu, D. Xing, Multi-material electrospinning: from methods to biomedical applications, Mater Today Bio 21 (2023) 100710.

[16] N. Siddiqui, S. Asawa, B. Birru, R. Baadhe, S. Rao, PCL-Based composite scaffold matrices for tissue engineering applications, Mol. Biotechnol. 60 (2018) 506–532.

[17] W. Pi, Y. Zhang, L. Li, C. Li, M. Zhang, W. Zhang, Q. Cai, P. Zhang, Polydopamine-coated polycaprolactone/carbon nanotube fibrous scaffolds loaded with brain-derived neurotrophic factor for peripheral nerve regeneration, Biofabrication 14 (2022).

[18] T.D. Stocco, M.C. Moreira Silva, M.A.F. Corat, G. Goncalves Lima, A.O. Lobo, Towards bioinspired meniscus-regenerative scaffolds: engineering a novel 3D bioprinted patient-specific construct reinforced by biomimetically aligned nanofibers, Int J Nanomedicine 17 (2022) 1111–1124.

[19] P. Ahmadi, N. Nazeri, M.A. Derakhshan, H. Ghanbari, Preparation and characterization of polyurethane/chitosan/CNT nanofibrous scaffold for cardiac tissue engineering, Int. J. Biol. Macromol. 180 (2021) 590–598.

[20] Y. Huang, L. Zhang, Y. Ji, H. Deng, M. Long, S. Ge, Y. Su, S.Y. Chan, X.J. Loh, A. Zhuang, J. Ruan, A non-invasive smart scaffold for bone repair and monitoring, Bioact. Mater. 19 (2023) 499–510.

[21] L. Hou, W. Wang, M.K. Wang, X.S. Song, Acceleration of healing in full-thickness wound by chitosan-binding bFGF and antimicrobial peptide modification chitosan membrane, Front. Bioeng. Biotechnol. 10 (2022) 878588.

[22] D. Guan, J. Mi, X. Chen, Y. Wu, Y. Yao, L. Wang, Z. Xiao, Y. Zhao, B. Chen, J. Dai, Lung endothelial cell-targeted peptide-guided bFGF promotes the regeneration after radiation induced lung injury, Biomaterials 184 (2018) 10–19.

[23] X. Zhang, X. Kang, L. Jin, J. Bai, W. Liu, Z. Wang, Stimulation of wound healing using bioinspired hydrogels with basic fibroblast growth factor (bFGF), Int J Nanomedicine 13 (2018) 3897–3906.

[24] Y. Liu, K. Ai, L. Lu, Polydopamine and its derivative materials: synthesis and promising applications in energy, environmental, and biomedical fields, Chem Rev 114 (2014) 5057–5115.

[25] A. Jin, Y. Wang, K. Lin, L. Jiang, Nanoparticles modified by polydopamine: working as "drug" carriers, Bioact. Mater. 5 (2020) 522–541.

[26] M.L. Alfieri, T. Weil, D.Y.W. Ng, V. Ball, Polydopamine at biological interfaces, Adv. Colloid Interface Sci. 305 (2022) 102689.

[27] M. Bao, K. Wang, J. Li, Y. Li, H. Zhu, M. Lu, Y. Zhang, Q. Fan, L. Han, K. Wang, D. Wang, Y. Gao, B. Peng, Z. Ming, W. Liu, ROS Scavenging and inflammation-directed polydopamine nanoparticles regulate gut immunity and flora therapy in inflammatory bowel disease, Acta Biomater. 161 (2023) 250–264.

[28] D. Cui, M. Li, P. Zhang, F. Rao, W. Huang, C. Wang, W. Guo, T. Wang, Polydopamine-coated polycaprolactone electrospun nanofiber membrane loaded with thrombin for wound hemostasis, Polymers 15 (2023).

[29] Z. Wu, K. Yuan, Q. Zhang, J.J. Guo, H. Yang, F. Zhou, Antioxidant PDA-PEG nanoparticles alleviate early osteoarthritis by inhibiting osteoclastogenesis and angiogenesis in subchondral bone, J. Nanobiotechnol. 20 (2022).

[30] W. Ma, X. Zhang, Y. Liu, L. Fan, J. Gan, W. Liu, Y. Zhao, L. Sun, Polydopamine decorated microneedles with Fe-MSC-derived nanovesicles encapsulation for wound healing, Adv. Sci. 9 (2022).

[31] M. Monavarian, S. Kader, S. Moeinzadeh, E. Jabbari, Regenerative scar-free skin wound healing, Tissue Eng Part B Rev 25 (2019) 294–311.

[32] X. Cao, L. Sun, Z. Luo, X. Lin, Y. Zhao, Aquaculture derived hybrid skin patches for wound healing, Engineered Regeneration 4 (2023) 28–35.

[33] X. Wang, B. Ding, G. Sun, M. Wang, J. Yu, Electro-spinning/netting: a strategy for the fabrication of three-dimensional polymer nano-fiber/nets, Prog. Mater. Sci. 58 (2013) 1173–1243.

[34] Y. Xu, Q. Saiding, X. Zhou, J. Wang, W. Cui, X. Chen, Electrospun fiber-based immune engineering in regenerative medicine, Smart Medicine 3 (2024).

[35] Y. Zhu, B. Kong, R. Liu, Y. Zhao, Developing biomedical engineering technologies for reproductive medicine, Smart Medicine 1 (2022).

[36] A.A. Mieloch, J.A. Semba, J.D. Rybka, CNT-Type dependent cellular adhesion on 3D-printed nanocomposite for tissue engineering, Int J Bioprint 8 (2022) 548.

[37] R. Balint, N.J. Cassidy, S.H. Cartmell, Conductive polymers: towards a smart biomaterial for tissue engineering, Acta Biomater. 10 (2014) 2341–2353.

[38] C. Jiang, K. Wang, Y. Liu, C. Zhang, B. Wang, Using wet electrospun PCL/Gelatin/CNT yarns to fabricate textile-based scaffolds for vascular tissue engineering, ACS Biomater. Sci. Eng. 7 (2021) 2627–2637.

[39] Y. Guo, Z. Hu, J. Chen, Z. Zhang, Q. Liu, J. Li, J. Yang, Z. Ma, J. Zhao, J. Hu, J. Wu, Z. Chen, Injectable TG-linked recombinant human collagen hydrogel loaded with bFGF for rat cranial defect repair, Int. J. Biol. Macromol. 236 (2023) 123864.

[40] T. Chen, Q. Zou, C. Du, C. Wang, Y. Li, B. Fu, Biodegradable 3D printed HA/CMCS/PDA scaffold for repairing lacunar bone defect, Mater Sci Eng C Mater Biol Appl 116 (2020) 111148.

[41] X. Fu, J. Wang, D. Qian, Z. Chen, L. Chen, W. Cui, Y. Wang, Living Electrospun short fibrous sponge via engineered nanofat for wound healing, Advanced Fiber Materials 5 (2022) 979–993.

[42] P. Zheng, B. Ding, G. Li, Polydopamine-incorporated nanoformulations for biomedical applications, Macromol. Biosci. 20 (2020) e2000228.

[43] M.R.A.P. Dethe, H. Ahmed, M. Agrawal, U. Roy, A. Alexander, PCL-PEG copolymer based injectable thermosensitive hydrogels, J Control Release 343 (2022) 217–236.

[44] M. Furtado, L. Chen, Z. Chen, A. Chen, W. Cui, Development of fish collagen in tissue regeneration and drug delivery, Engineered Regeneration 3 (2022) 217–231.

[45] Y. Fu, L. Yang, J. Zhang, J. Hu, G. Duan, X. Liu, Y. Li, Z. Gu, Polydopamine antibacterial materials, Mater. Horiz. 8 (2021) 1618–1633.

[46] C.M. Ho, A. Mishra, P.T. Lin, S.H. Ng, W.Y. Yeong, Y.J. Kim, Y.J. Yoon, 3D Printed polycaprolactone carbon nanotube composite scaffolds for cardiac tissue engineering, Macromol. Biosci. 17 (2017).

[47] S. Mombini, J. Mohammadnejad, B. Bakhshandeh, A. Narmani, J. Nourmohammadi, S. Vahdat, S. Zirak, Chitosan-PVA-CNT nanofibers as

electrically conductive scaffolds for cardiovascular tissue engineering, Int. J. Biol. Macromol. 140 (2019) 278–287.
[48] S.M. Mousavi, K. Yousefi, S.A. Hashemi, M. Afsa, I.S. Bahran, A. Gholami, Y. Ghahramani, A. Alizadeh, W.H. Chiang, Renewable carbon nanomaterials: novel resources for dental tissue engineering, Nanomaterials 11 (2021).
[49] Y. Xiong, B.-B. Mi, Z. Lin, Y.-Q. Hu, L. Yu, K.-K. Zha, A.C. Panayi, T. Yu, L. Chen, Z.-P. Liu, A. Patel, Q. Feng, S.-H. Zhou, G.-H. Liu, The role of the immune microenvironment in bone, cartilage, and soft tissue regeneration: from mechanism to therapeutic opportunity, Military Medical Research 9 (2022).
[50] M.S. Kim, G. Kim, Three-dimensional electrospun polycaprolactone (PCL)/alginate hybrid composite scaffolds, Carbohydr. Polym. 114 (2014) 213–221.
[51] Y. Zhang, H. Ouyang, C.T. Lim, S. Ramakrishna, Z.M. Huang, Electrospinning of gelatin fibers and gelatin/PCL composite fibrous scaffolds, J. Biomed. Mater. Res. B Appl. Biomater. 72 (2005) 156–165.